Structural Characteristics of Synthetic Amorphous Calcium Carbonate

F. Marc Michel,*[,†,‡] Jason MacDonald,[†,‡] Jian Feng,[†,§] Brian L. Phillips,[†,‡] Lars Ehm,[‡] Cathy Tarabrella,[‡] John B. Parise,[†,‡,§] and Richard J. Reeder[†,‡]

Center for Environmental Molecular Science, Department of Geosciences, and Department of Chemistry, Stony Brook University, Stony Brook, New York 11794

Received January 31, 2008. Revised Manuscript Received April 18, 2008

Amorphous calcium carbonate (ACC) is an important phase involved in calcification by a wide variety of invertebrate organisms and is of technological interest in the development of functional materials. Despite widespread scientific interest in this phase a full characterization of structure is lacking. This is mainly due to its metastability and difficulties in evaluating structure using conventional structure determination methods. Here we present new findings from the application of two techniques, pair distribution function analysis and nuclear magnetic resonance spectroscopy, which provide new insight to structural aspects of synthetic ACC. Several important results have emerged from this study of ACC formed in vitro using two common preparation methods: (1) ACC exhibits no structural coherence over distances > 15 Å and is truly amorphous; (2) most of the hydrogen in ACC is present as structural H_2O, about half of which undergoes restricted motion on the millisecond time scale near room temperature; (3) the short- and intermediate-range structure of ACC shows no distinct match to any known structure in the calcium carbonate system; and (4) most of the carbonate in ACC is monodentate making it distinctly different from monohydrocalcite. Although the structure of synthetic ACC is still not fully understood, the results presented provide an important baseline for future experiments evaluating biogenic ACC and samples containing certain additives that may play a role in stabilization of ACC, crystallization kinetics, and final polymorph selection.

1. Introduction

The role of an amorphous precursor in the formation of crystalline calcium carbonate phases has become the focus of study among several research communities. It is now known that a surprising number of calcifying invertebrate organisms initially form an amorphous calcium carbonate (ACC) phase, which subsequently crystallizes to form skeletal parts, some with intricate architecture. Final crystalline phases are typically the mineral forms of $CaCO_3$: calcite or aragonite. Biological control over the selection of mineral form and morphology indicates complex interactions between the organism and the ACC precursor, which are not fully understood. Such biomineralization has inspired the design of functional calcium carbonate phases or composites that may only be formed using an amorphous precursor, with subsequent crystallization.[1,2] Functionalized templates may be used to direct assembly to obtain thin films or selected morphologies or orientations of crystalline calcium carbonate. A distinct advantage of an amorphous precursor is the ability to create and store a metastable material—with far greater density and stability than a supersaturated solution—that can be induced to transform into a more stable phase with only modest changes in volume and energy.

Effective application of the amorphous calcium carbonate pathway for development of functional materials requires an understanding of the principal factors that provide temporary stabilization of the amorphous phase, that direct assembly, and that govern selection of the final crystalline polymorph (aragonite or calcite). Different forms of ACC have been recognized among biogenic and synthetic samples.[3–5] These have been distinguished on the basis of their stability, or rate at which they transform to a crystalline phase. Some biogenic ACC is found to be inherently unstable and transforms readily; these so-called transient forms are largely anhydrous.[3,4] Other biogenic forms, as well as most synthetic ACC, may persist for days to weeks without undergoing transformation and have been called stable.[3] The term "stable" has been widely adopted to distinguish this material from even less stable forms (i.e., transient) that transform without delay. Since the so-called stable form of ACC is understood to be metastable on different time scales it will hereinafter be referred to as "stabilized". In biogenic ACC, the presence of inorganic and organic impurities, as well as

* Corresponding author. Current address: Department of Geological & Environmental Sciences, Stanford University, Stanford, California 94305.
† Center for Environmental Molecular Science, Stony Brook University.
‡ Department of Geosciences, Stony Brook University.
§ Department of Chemistry, Stony Brook University.
|| Current address: National Synchrotron Light Source, Brookhaven National Laboratory, Upton, New York 11973 and Mineral Physics Institute, Stony Brook University, Stony Brook, New York 11794.

(1) Aizenberg, J.; Muller, D. A.; Grazul, J. L.; Hamann, D. R. *Science* **2003**, *299* (5610), 1205–1208.
(2) Dujardin, E.; Mann, S. *Adv. Mater.* **2002**, *14* (11), 775–788.
(3) Addadi, L.; Raz, S.; Weiner, S. *Adv. Mater.* **2003**, *15* (12), 959–970.
(4) Raz, S.; Hamilton, P. C.; Wilt, F. H.; Weiner, S.; Addadi, L. *Adv. Funct. Mater.* **2003**, *13* (6), 480–486.
(5) Weiner, S.; Levi-Kalisman, Y.; Raz, S.; Addadi, L. *Connect. Tissue Res.* **2003**, *44*, 214–218.

10.1021/cm800324v CCC: $40.75
Published on Web 06/27/2008

structural water in stabilized ACC varieties, suggests that these components likely play important roles in temporarily stabilizing ACC and in controlling the crystallization kinetics and identity of the final product.[3] Among inorganic components, magnesium and phosphate are thought to be most important, whereas a wide range of organic components may be involved.[6–8] Inasmuch as natural biogenic ACC contains complex admixtures of many foreign components, these materials do not lend themselves to evaluation of the function of individual additives. Consequently, much attention has been focused on laboratory synthesis of ACC, where proper experimental design can facilitate assessment of individual factors that control metastability, crystallization kinetics, and polymorph selection. The primary factor that links the function of additives to the properties and behavior of the ACC is the structure of the amorphous phase. Structure of the ACC is also expected to constrain its interaction with functional groups and molecules in organic templates that may direct assembly. Furthermore, changes in local structure that accompany the transformation of ACC to a crystalline form may control the concentration of retained impurities, which could affect function. This also has implications for geochemical applications relying on trace metal contents. One example is the wide use of Mg and Sr concentrations in the buried fossil remains of calcifying invertebrates to infer paleo-oceanographic and paleo-climatic trends over time.

Structural characterization of ACC has been hindered by its amorphous-like nature, small particle size, and metastable behavior. Powder X-ray diffraction (XRD) of laboratory synthesized ACC typically shows up to two diffuse, broad maxima, which excludes the use of conventional structure determination methods. The apparent absence of long-range order has led to the use of local structural probes, such as X-ray absorption spectroscopy (XAS) and FTIR spectroscopy, for characterization of short-range structure in ACC. Ca K-edge extended X-ray absorption fine structure (EXAFS) studies [9,10] have primarily given information limited to the first coordination sphere of Ca, as shown by a single peak in Fourier transforms, with evidence of more distant shells limited to a few varieties.[11] EXAFS fit results show differences in the Ca−O distance and number of coordinating oxygen atoms for ACC samples taken from different organisms and produced in laboratory syntheses (Supporting Information, Text-1). In several studies Ca−O distances of approximately 2.40−2.42 Å are reported for stabilized ACC, which are similar to the average Ca−O distance in monohydrocalcite.[12] Such similarities raise the possibility that some ACC is actually a nanocrystalline phase and not amorphous. Although X-ray absorption spectroscopy provides important constraints on local coordination, it provides little or no structural information over greater length scales.

Whereas transient ACC is largely anhydrous, thermogravimetric analysis (TGA) has shown that stabilized ACC varieties typically contain up to ∼15 wt % H_2O (e.g., refs 7, 13, and 14); this value corresponds to a formula $CaCO_3 \cdot H_2O$, which is also the formula of monohydrocalcite. Hence, monohydrocalcite has been a convenient starting model for investigation of structural properties of stabilized ACC samples.[3,7,15] Upon transformation of stabilized ACC to a crystalline form the H_2O is lost. FTIR confirms the presence of hydrous components in stabilized ACC,[9] with an intense broad feature at 3500−3200 cm^{-1}, but provides no insight to their coordination or function. FTIR studies also reveal features that distinguish ACC from crystalline calcium carbonate (Supporting Information, Text-2). Despite the distinctive features of ACC observed in IR spectra, only limited insight to ACC structure has been gained from this spectroscopic technique.

In the present paper we report findings obtained from application of two techniques, pair distribution function (PDF) analysis and nuclear magnetic resonance (NMR) spectroscopy, that provide new insight to structural aspects of synthetic ACC. This initial report focuses on additive-free ACC and provides a baseline for evaluation of biogenic samples as well as ACC samples containing additives. The PDF analysis is derived from high-energy X-ray total scattering data and provides the first evidence for medium-range structure in ACC and confirms its amorphous character. The ^{13}C and ^{1}H NMR data provide the first evidence for the structural role of water and the first constraints on the identity and linkage of the CO_3 units in synthetic ACC. Combined with XAS and FTIR data, these new findings provide a more complete characterization of synthetic ACC than previously known. The new findings show that these complementary techniques will prove essential for assessing structure in ACC containing additives, as well as for characterizing the pathway of the transformation of ACC to crystalline forms.

2. Experimental Section

2.1. Synthesis of Amorphous Calcium Carbonate. Two different methods were used to synthesize ACC in this study. Method I was adapted from the procedure described by Koga et al.,[14] in which calcium chloride and sodium carbonate solutions, equimolar in Ca and CO_3, were rapidly mixed. In this method 106 mg of solid sodium carbonate was added to 20 mL of a 0.5 M sodium hydroxide solution and 30 mL of deionized water. This solution was combined with 50 mL of a 20 mM calcium chloride solution and stirred rapidly, followed immediately by vacuum filtration and rinsing with acetone to dry the solid. Samples for NMR analysis were prepared from sodium carbonate enriched to 99% in ^{13}C. Method II was derived from the procedure described by Faatz et al.[13] and differed primarily from method I by use of dimethyl carbonate as the CO_3 source. This method involves addition of 147

(6) Aizenberg, J.; Lambert, G.; Weiner, S.; Addadi, L. *J. Am. Chem. Soc.* **2002**, *124* (1), 32–39.
(7) Levi-Kalisman, Y.; Raz, S.; Weiner, S.; Addadi, L.; Sagi, I. *J. Chem. Soc., Dalton Trans.* **2000**, (21), 3977–3982.
(8) Loste, E.; Diaz-Marti, E.; Zarbakhsh, A.; Meldrum, F. C. *Langmuir* **2003**, *19* (7), 2830–2837.
(9) Becker, A.; Bismayer, U.; Epple, M.; Fabritius, H.; Hasse, B.; Shi, J. M.; Ziegler, A. *Dalton Trans.* **2003**, (4), 551–555.
(10) Levi-Kalisman, Y.; Raz, S.; Weiner, S.; Addadi, L.; Sagi, I. *Adv. Funct. Mater.* **2002**, *12* (1), 43–48.
(11) Politi, Y.; Levi-Kalisman, Y.; Raz, S.; Wilt, F.; Addadi, L.; Weiner, S.; Sagi, I. *Adv. Funct. Mater.* **2006**, *16* (10), 1289–1298.
(12) Effenberger, H. *Monatsh. Chem.* **1981**, *112* (8−9), 899–909.
(13) Faatz, M.; Grohn, F.; Wegner, G. *Adv. Mater.* **2004**, *16* (12), 996–1000.
(14) Koga, N.; Nakagoe, Y. Z.; Tanaka, H. *Thermochim. Acta* **1998**, *318* (1−2), 239–244.
(15) Lam, R. S. K.; Charnock, J. M.; Lennie, A.; Meldrum, F. C. *Crystengcomm* **2007**, *9* (12), 1226–1236.

mg of solid calcium chloride dihydrate and 450 mg of dimethyl carbonate to 80 mL of deionized water, followed by addition of 20 mL of 0.5 M sodium hydroxide solution. This mixture was stirred for approximately 2.5 min, and the solid precipitate was vacuum-filtered and dried with acetone. Both methods were conducted at room temperature in open air.

2.2. Reference Samples. Reference samples of well-crystallized calcite ($CaCO_3$), aragonite ($CaCO_3$), vaterite ($CaCO_3$), portlandite ($Ca(OH)_2$), and monohydrocalcite ($CaCO_3 \cdot H_2O$) were also evaluated as part of this study. A reagent grade sample of calcite was obtained from Spectrum Chemicals and portlandite (EXAFS only) from Alfa Aesar. Synthetic aragonite was prepared at room temperature in a supersaturated calcium carbonate solution containing Mg^{2+} in the ratio Mg:Ca 7:1. Synthetic samples of vaterite and monohydrocalcite were formed according to established preparation methods. The synthetic monohydrocalcite contained minor impurities of aragonite or calcite. The monohydrocalcite evaluated by NMR is a natural specimen from the Maricopa Mountains of Arizona, where it occurs as brown fine-grained sand from decomposition of weddellite in decaying cacti.

2.3. X-ray Absorption Spectroscopy. Extended X-ray absorption fine structure (EXAFS) and X-ray absorption near-edge structure (XANES) spectra were collected at the Ca K-edge for both ACC samples and for selected reference compounds at the bending magnet beamline 20-BM at the Advanced Photon Source (APS) at Argonne National Laboratory (ANL). The ACC samples were prepared according to methods I and II and XAS data collection started within < 0.5 h of synthesis. All spectra were collected in transmission mode at room temperature. Additional details are included in Supporting Information, Text-3.

2.4. High-Energy X-ray Total Scattering and Pair Distribution Function Analysis. High energy X-ray total scattering data were collected at the 1-ID beamline (~100 keV, $\lambda = 0.1240(6)$ Å)[16] at the Advanced Photon Source (APS) at Argonne National Laboratory (ANL). The ACC samples were prepared on-site according to methods I and II and the collection of total scattering data commenced < 1 h from the time of synthesis. A CeO_2 standard (NIST diffraction intensity standard set: 674a) was used to calibrate the sample-to-detector distance and the nonorthogonality of the detector relative to the incident beam path. The radiation scattered by the calibrant and samples was collected on an amorphous Si detector system manufactured by General Electric. Conversion of data from 2D to 1D was done using the program Fit-2D.[17,18] A polarization correction was applied during integration of the data.

The experimental total scattering structure function $S(Q)$, reduced experimental structure function $f(Q)$, and PDF, or $G(r)$, were obtained using PDFgetX2[19] where standard corrections were applied as well as those unique to image-plate geometry.[20] The composition used in the normalization of each experimental structure function was $CaCO_3 \cdot H_2O$. The PDFs for both ACC samples (methods I and II) were calculated from the Fourier transform of the reduced structure function truncated at ~26 $Å^{-1}$. The PDFs for vaterite, aragonite, monohydrocalcite, and calcite reference structures were calculated using the program DiffPy[21] and based on the structural parameters reported in the Inorganic Crystal Structure Database (ICSD) as entries 15879, 52152, 100846, and 40107, respectively.

2.5. NMR Techniques. All solid-state NMR spectra were collected on a 400 MHz (9.4 T) Varian Inova spectrometer operating at 100.6 MHz for ^{13}C and 399.76 MHz for ^{1}H. $^{13}C\{^{1}H\}$ two-dimensional heteronuclear correlation (HETCOR) NMR spectra[22] were obtained using a Varian/Chemagnetics "T3" probe assembly configured for 3.2 mm (outer diameter) thin wall rotors. The HETCOR spectra were acquired at 10 kHz spinning rate with 1 s acquisition delay and a linear ramp of the ^{13}C B_1 field during contact time. To stabilize the initial ACC, the sample was dried in vacuum for 30 min after being loaded into the rotor, which was then sealed. ^{13}C single pulse magic angle spinning (SP/MAS) NMR spectra and $^{13}C\{^{1}H\}$ CP/MAS NMR spectra acquired before and after each HETCOR experiment showed no changes, indicating that no transformation occurred during the HETCOR acquisition. ^{1}H MAS NMR spectra were obtained under similar experimental conditions. $^{13}C\{^{1}H\}$ CP kinetics were measured with a Varian/Chemagnetics "T3" probe assembly configured for 7.5 mm (outer diameter) rotors. The experimental conditions set for $^{13}C\{^{1}H\}$ CP/MAS NMR were 3 kHz spinning rate, 8 μs 90° ^{1}H excitation pulse, 1 s acquisition delay, and 32 kHz spin-locking (CW mode) power for both ^{13}C and ^{1}H channels during contact time. For quantitative comparison, ^{13}C SP/MAS NMR spectrum was obtained at 3 kHz spinning rate, with 8 μs 90° excitation pulse and 1 h acquisition delay due to the long spin−lattice relaxation time of ^{13}C.

2.6. X-ray Diffraction Methods. XRD data for freshly prepared ACC samples mounted as powders on glass slides were collected using a Scintag PADx diffractometer equipped with Cu Kα radiation (λ = ~1.5415 Å) and a solid-state Ge detector.

2.7. FTIR Methods. Fourier transform infrared spectroscopy (FTIR) was performed using a Thermo Electron Nicolet Nexus 670 instrument. Freshly prepared ACC samples were mixed with dry KBr in a 1:10 ratio within < 0.5 h of synthesis. Diffuse reflectance spectra were obtained using a MCT detector. Spectra are presented after subtraction of the corresponding KBr spectrum.

2.8. TGA Methods. TGA of ACC samples prepared according to methods I and II commenced within < 0.5 h of synthesis. TGA was carried out using a Netzsch STA 449C Jupiter instrument with flowing air over the range of 25 to 800 °C, with a heating rate of 5 °/min. ACC samples were loaded into Al_2O_3 sample cups immediately after synthesis. For the ACC sample synthesized using the sodium carbonate source, one-half of the product was stored in a vacuum desiccator for approximately 5 h under soft vacuum prior to measurement.

3. Results and Discussion

3.1. Sample Characterization. Initial characterization of laboratory synthesized ACC involved using standard methods of powder XRD, FTIR, and TGA. XRD patterns for freshly synthesized ACC show two broadened and diffuse maxima (Supporting Information, Figure S1) that do not correspond to strongest diffraction lines of either calcite or aragonite

(16) Shastri, S. D.; Fezzaa, K.; Mashayekhi, A.; Lee, W.-K.; Fernandez, P. B.; Lee, P. L. *J. Synchrotron Radiat.* **2002**, (9), 317–322.
(17) Hammersley, A. P., *"Fit2D" V. 9.129 Reference Manual*, Version 3.1; ESRF Internal Report, ESRF98HA01T; 1998. http://www.esrf.eu/computing/scientific/FIT2D/FIT2D_REF/node268.html.
(18) Hammersley, A. P.; Svenson, S. O.; Hanfland, M.; Hauserman, D. *High Pressure Res.* **1996**, *14*, 235–248.
(19) Qiu, X.; Thompson, J. W.; Billenge, S. J. L. *J. Appl. Crystallogr.* **2004**, *37*, 678.
(20) Chupas, P. J.; Qui, X.; Hanson, J. C.; Lee, P. L.; Grey, C. P.; Billinge, S. J. L. *J. Appl. Crystallogr.* **2003**, *36*, 1342–1347.
(21) Farrow, C. L.; Juhas, P.; Liu, J. W.; Bryndin, D.; Bozin, E. S.; Bloch, J.; Proffen, T.; Billinge, S. J. L. *J. Phys.: Condens. Matter* **2007**, *19*, 335219.
(22) Schmidtrohr, K.; Clauss, J.; Spiess, H. W. *Macromolecules* **1992**, *25* (12), 3273–3277.

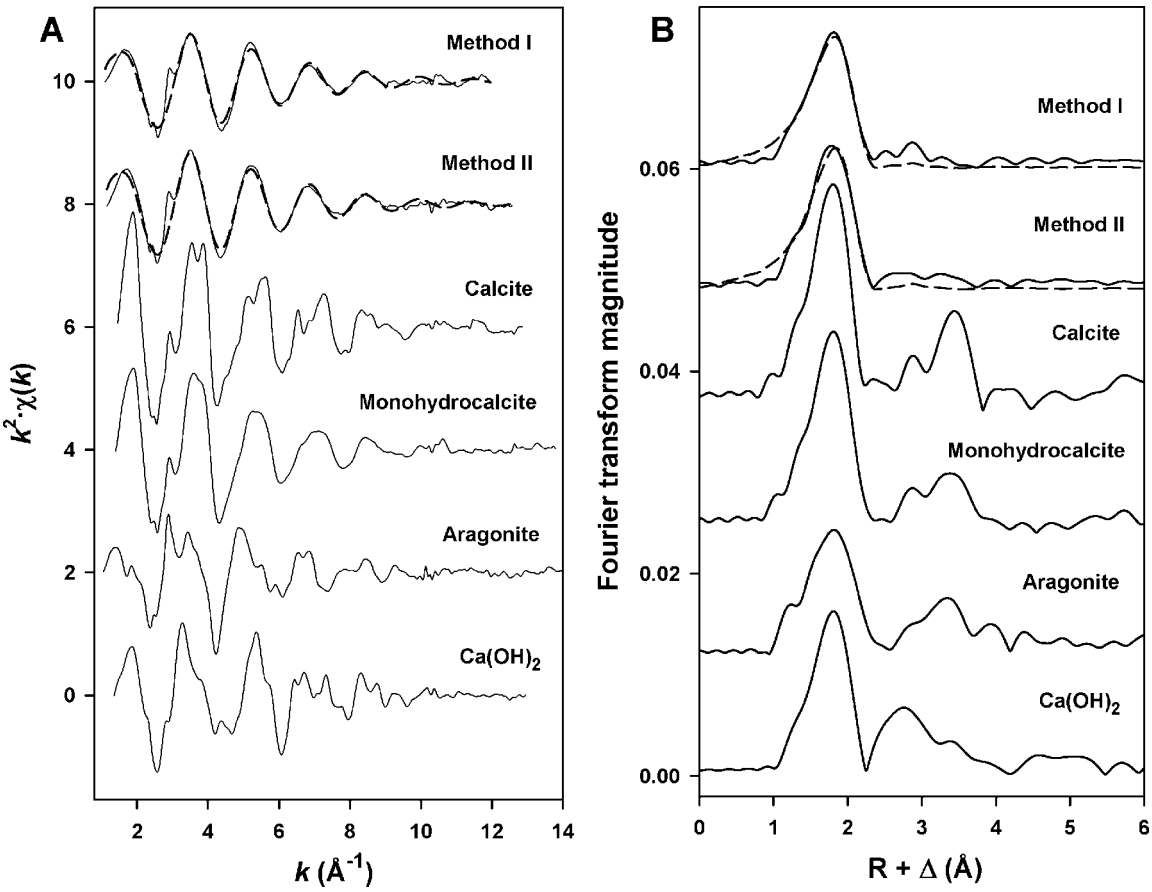

Figure 1. A and B. Ca K-edge EXAFS function (pane A) obtained from data collected immediately after synthesis of ACC using methods I and II. The calculated Fourier transform (FT) magnitudes (not corrected for phase shifts) are shown for both ACC samples as well as for the four reference samples (pane B). The fits for χ and the FT magnitudes are overlain (black dashes). The strong peak observed at ~1.8 Å in the FT magnitudes of the ACC samples corresponds to the distance between calcium and oxygen, which is fit at ~2.4 Å. Sharp features in the EXAFS at 2.4, 2.9, and 10.4 $Å^{-1}$ correspond to multielectron excitations.

and are consistent with those reported in prior studies (e.g., refs 13 and 23). FTIR of freshly prepared ACC reveals several features that distinguish it from crystalline calcite (Supporting Information, Figure S2). The broad feature between 3500−3200 cm^{-1} confirms the presence of hydrous components in ACC. Additional features include the ν_2, ν_3, and ν_4 internal modes of the CO_3 group at ~870, 1420−1475, and ~713 cm^{-1}, respectively, and are consistent with previous studies (e.g., refs 3, 6, and 23). TGA of freshly prepared ACC shows smooth weight loss up to ~400 °C (Supporting Information, Text-4 and Figure S3). The weight loss observed from the start of each experiment to the temperature at which the samples became anhydrous (average mass between 300 − 400 °C) totals 17.6% and 19.9% and corresponds to H_2O:$CaCO_3$ ratios of 1.38 and 1.19 for methods I and II, respectively. Above ~600 °C, dramatic weight loss occurs due to the loss of CO_2 during the thermal decomposition of calcium carbonate. While these methods combined provide partial information regarding composition and the means to identify ACC, they provide only limited insight into the structure of this phase.

3.2. X-ray Absorption Spectroscopy. The EXAFS χ curves for the ACC samples show a single beat (Figure 1A), consistent with a single peak in the Fourier transforms (Figure 1B). The sharp features at 2.4, 2.9, and 10.4 $Å^{-1}$ in the χ curves are associated with multielectron excitations and likely have little influence on fit results.[24] Fourier transform magnitudes for both ACC samples are dominated by a single peak fitted as oxygen atoms at $R_{Ca-O} = 2.41(2)$ Å. Best fit coordination number (CN) values are 6.7 and 6.1 (±25%) for ACC synthesized by methods I and II, respectively. The Debye−Waller factor, σ^2 equals 0.010 $Å^2$, is strongly correlated with CN and the amplitude reduction factor S_o^2. Weak features in the FT magnitude from 2.5−3.4 $Å^{-1}$ are not reliably fit with O, C, or Ca shells. The single peak seen for the ACC samples is significantly broader and lower in amplitude than the peak corresponding to first-shell O atoms in the FTs for calcite and monohydrocalcite. Complete fit results are shown in Supporting Information, Table S1.

Normalized XANES spectra for both ACC samples are shown along with spectra for reference compounds in Figure 2. Edge structures for both ACC samples are the same but are distinct from those of the reference compounds shown. The ACC shows a single broad white line without the splitting seen in the calcite or the pronounced shoulders seen on the high-energy side of the white line for aragonite and $Ca(OH)_2$. The shoulder on the low-energy side of the ACC

(23) Gunther, C.; Becker, A.; Wolf, G.; Epple, M. *Z. Anorg. Allg. Chem.* **2005**, *631* (13−14), 2830–2835.

(24) Fulton, J. L.; Chen, Y. S.; Heald, S. M.; Balasubramanian, M., *J. Chem. Phys.* **2006**, *125* (9), 094507 (10 pages).

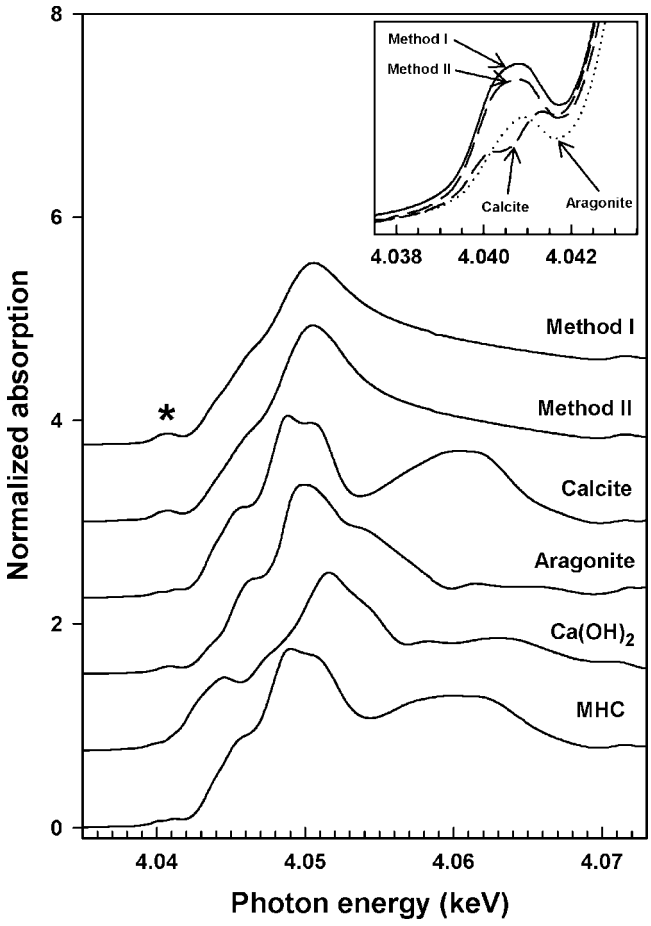

Figure 2. XANES spectra collected immediately after synthesis of ACC using methods I and II compared to spectra for four reference samples: calcite, aragonite, $Ca(OH)_2$, and monohydrocalcite (MHC). The * indicates the position of a pre-edge feature, which is expanded in the inset.

white line (4044−4046 eV) is less pronounced than in the reference compounds, where it has been attributed to the 1s → 4p transition.[25] A pre-edge feature at 4040−4041 eV (indicated by * in Figure 2) is noticeably more intense in the ACC than in the reference compounds. This peak is attributable to the 1s → 3d transition. This transition is forbidden in octahedral symmetries although weak intensity may exist as a result of thermal disorder or quadrupolar coupling.[25] Closer examination of this region of the XANES (Figure 2, inset) shows single peaks for ACC and aragonite, with significantly greater intensity for the ACC samples. The calcite feature appears as a doublet of weak intensity approximately centered around the mid position of the peaks of the other samples. In calcite the Ca atom is centered in a near regular octahedron, whereas in aragonite the Ca atom occupies a 9-fold site. From the greater intensity of the peak from the ACC samples, we may infer that its first-shell coordination is significantly distorted relative to an octahedron, and perhaps also relative to the coordination in aragonite. While XAS studies of ACC provide detailed information regarding the local coordination environment of Ca, there is little or no reliable information obtainable beyond the first coordination shell. In the case of EXAFS this is

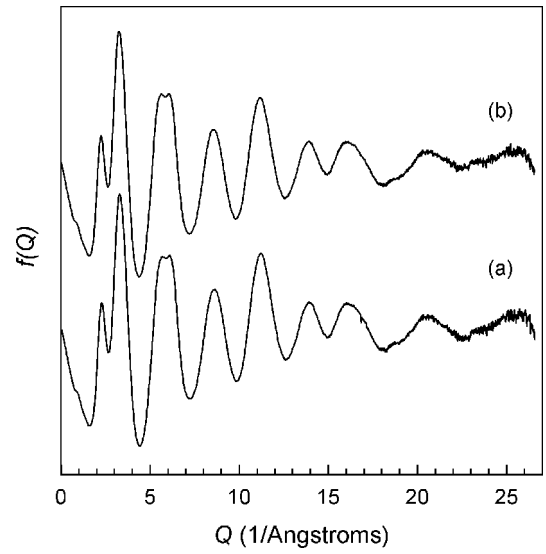

Figure 3. Experimental reduced structure functions $f(Q)$ of ACC collected immediately after synthesis using methods I (a) and II (b). The patterns are virtually identical over a Q-range of ~26 $Å^{-1}$. The FSDP at 2.2 $Å^{-1}$ indicates the presence of intermediate-range ordering.

obvious in that there are usually no features observed beyond the first peak in the FT magnitude, except in select samples of transient ACC. This has hindered the development of a structural model for ACC because there is no strong evidence regarding the connectivity of the Ca−O polyhedra to neighboring polyhedra in the structure.

3.3. X-ray Total Scattering and PDF Analysis of ACC. Comparison of the experimental structure functions $f(Q)$ for the initial ACC prepared by methods I and II indicates that their atomic arrangements are virtually identical (Figure 3). Although the features observed in $f(Q)$ are in general characterized by broad maxima, indicating the absence of long-range periodicity, the occurrence of the first sharp diffraction peak (FSDP) at $Q = \sim 2.2$ $Å^{-1}$ suggests the presence of intermediate-range order in ACC.[26] Such features are commonly observed in tetrahedral glasses such as SiO_2[27] as well as other amorphous solids.[26,28,29] The PDFs for the ACC samples (Figure 4), obtained by Fourier transformation of $f(Q)$, are also virtually indistinguishable from one another but contain unique and additional structural information relative to EXAFS. The most striking overall feature is the rapid attenuation of the PDFs indicating the loss of structural coherence beyond ~15 Å. This result shows that the initial ACC exhibits only short-range and limited intermediate-range ordering, and therefore can be considered truly amorphous. The sharpest peaks in the PDFs occur at low-r (e.g., 1.3 and ~2.4 Å) and contain information on the first neighbor coordination environments around carbon and calcium, the basic structural units present. The prominent feature at ~2.4 Å (Figure 4) is related to the average Ca−O bond distance and is consistent with EXAFS analysis of ACC

(25) Fulton, J. L.; Heald, S. M.; Badyal, Y. S.; Simonson, J. M. *J. Phys. Chem. A* **2003**, *107* (23), 4688–4696.

(26) Susman, S.; Price, D. L.; Volin, K. J.; Dejus, R. J.; Montague, D. G. *J. Non-Cryst. Solids* **1988**, *106* (1−3), 26–29.

(27) Price, D. L.; Moss, S. C.; Reijers, R. *J. Phys.: Condens. Matter* **1989**, *1*, 1005–1008.

(28) Benmore, C. J.; Hart, R. T.; Mei, Q.; Price, D. L.; Yarger, J.; Tulk, C. A.; Klug, D. D. *Phys. Rev. B* **2005**, *72* (13), 132201 (4 pages).

(29) Wilding, M. C.; Benmore, C. J. *Rev. Mineral. Geochem.* **2006**, *63*, 275–311.

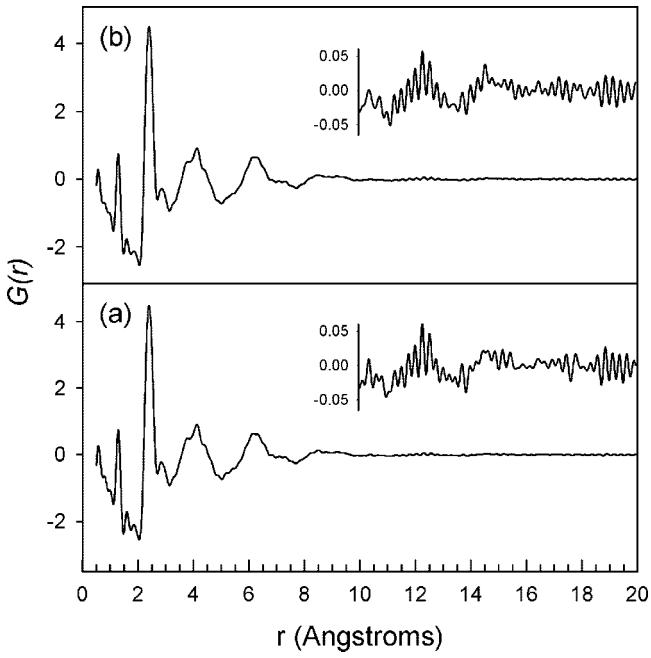

Figure 4. Pair distribution functions (PDF) calculated from the experimental reduced structure functions shown in Figure 3 for ACC. The average range of structural coherence is less than ~15 Å for the samples synthesized using either Method I (a) or Method II (b). Insets show expanded vertical scale over 10−20 Å.

presented above and elsewhere.[9,10,23,30] Beyond the first few distinct features in the PDF are relatively broad and less well-defined features occurring at approximately 4.0, 6.2, 8.5, 9.5, and 12.0 Å. Since an amorphous material inherently contains static disorder, it is not surprising that these features are less well resolved in the PDF. We note that the features beyond ~10 Å in the PDFs for ACC are extremely small and may be artifacts related to the Fourier transformation.

ACC exhibits ordering over a length scale less than 15 Å and therefore it is not practical to describe the structure of ACC using the conventional approach of replicating a unit cell, as is common for well-crystallized and even nanocrystalline materials.[31,32] However, it is possible to test whether the observed pair correlations in ACC are consistent with any of the known structures in the calcium carbonate system. Figure 5 shows a comparison of the PDF for ACC to the calculated PDFs for the structures of calcite, vaterite, aragonite, and monohydrocalcite. From this comparison several observations can be made: (1) the C−O distance for carbonate (~1.3 Å) is virtually identical in all structures; (2) the correlation for the first coordination shell of Ca in ACC (~2.4 Å) is most similar in terms of position to vaterite and monohydrocalcite; (3) the small peak observed at ~2.9 Å in ACC is similar to correlations present in aragonite, monohydrocalcite, and vaterite but not calcite; and (4) the broad correlations in ACC at ~4.0 and ~6.0 Å are similar in distance to correlations in all four of the reference structures. In general, comparison of the PDF for ACC to those of the reference compounds suggests some common correlations in the higher-r region (e.g., at ~4.0 and ~6.0 Å) that are likely dominated by Ca···x pairs (where x = Ca, O, and C), based primarily on the scattering power of these pairs of atoms. Despite the above-stated similarities, the short- and intermediate-range structure of ACC differs from that of each of these crystalline calcium carbonate phases.

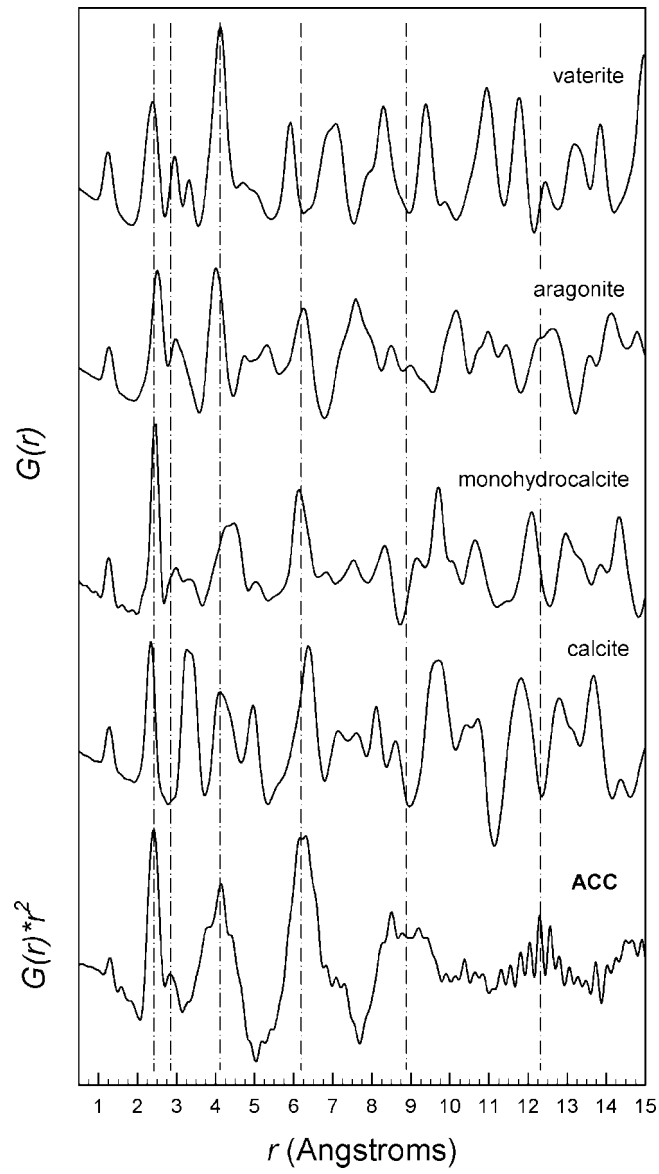

Figure 5. A comparison of the PDF for ACC to PDFs for four calcium carbonate phases. ACC is scaled as $G(r) \times r^2$ to amplify the weak correlations > ~10 Å. The PDFs for calcite and monohydrocalcite are experimental. The PDFs for vaterite and aragonite were calculated based on the structural parameters provided in ICSD nos. 15879 and 52152, respectively. Vertical dashed lines indicate positions of the most distinct features in ACC.

The pair correlations observed in ACC at ~4.0 and ~6.0 Å in the PDFs are notably absent in the EXAFS FT magnitudes (Figure 1) and have not been observed in previous Ca K-edge EXAFS studies. If these correlations in the PDFs represent Ca···x pairs, possible explanations for the absence of additional peaks in the FT may involve destructive interference of backscattering waves and/or inadequate range in k-space. One important advantage of

(30) Neumann, M.; Epple, M. *Eur. J. Inorg. Chem.* **2007**, (14), 1953–1957.
(31) Michel, F. M.; Antao, S. M.; Chupas, P. J.; Lee, P. L.; Parise, J. B.; Schoonen, M. A. A. *Chem. Mater.* **2005**, *17* (25), 6246–6255.
(32) Michel, F. M.; Ehm, L.; Antao, S. M.; Lee, P. L.; Chupas, P. J.; Liu, G.; Strongin, D. R.; Schoonen, M. A. A.; Phillips, B. L.; Parise, J. B. *Science* **2007**, *316* (5832), 1726–1729.

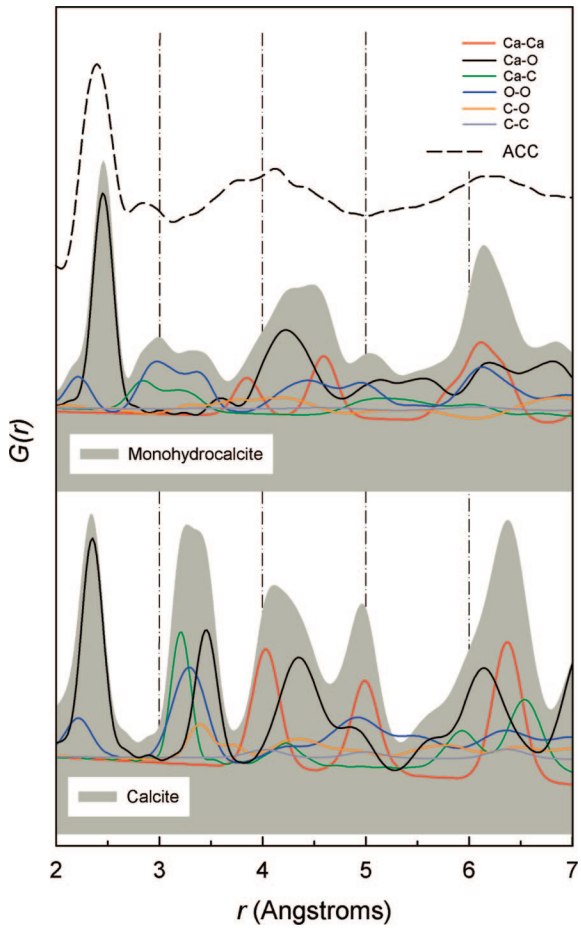

Figure 6. Calculated total PDFs for calcite (bottom gray fill) and monohydrocalcite (top gray fill) overlain with the partial PDFs for the six pairs of atoms in each structure (solid curves). Correlations relating to H are not included for monohydrocalcite.

X-ray total scattering and PDF analysis over EXAFS is that it represents the total electron density of a material. The ab initio extraction of a complete structural model from the PDF, however, is complicated by the additional information regarding all pairs of atoms in the material. This is illustrated in Figure 6, which shows the calculated total PDF for calcite and the individual pair correlations (or partials) for Ca−Ca, Ca−O, Ca−C, O−O, C−O, and C−C that contribute to the total PDF. The feature at ~2.4 Å in the PDF for calcite includes both Ca−O and O−O pair correlations and is relatively easy to interpret. However, the correlation for calcite at ~3.4 Å is the sum of the contributions from four pairs of atoms in the structure. This example for calcite illustrates how the correlations at greater *r*-values become increasingly complex due to overlapping contributions from a greater number of pairs. The assignment of these contributions is possible for the crystalline calcium carbonates because their structures are known (Figure 6 and Supporting Information, Figure S4). In the case of ACC, for which no structure model exists, the assignment of pair correlations is substantially more complex. Furthermore, although the PDF provides information regarding the total electron density of ACC, it becomes somewhat limited for evaluating the role of light and weakly scattering elements such as hydrogen.

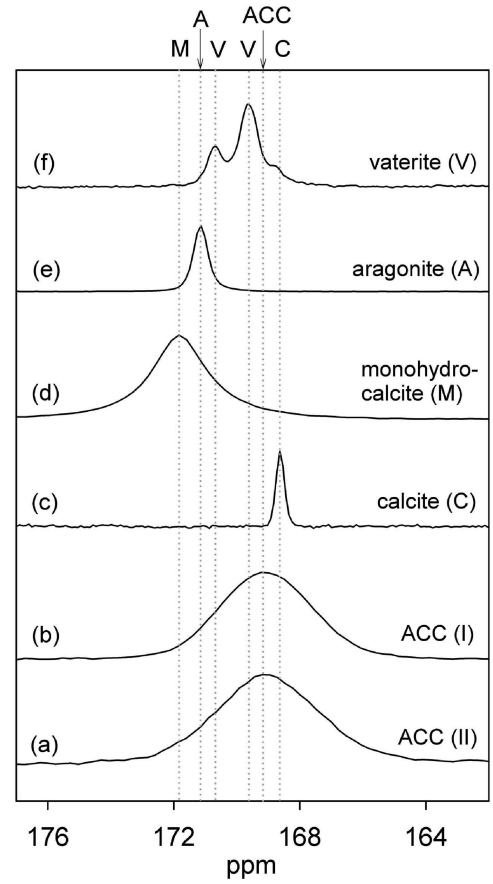

Figure 7. ^{13}C NMR spectra of calcium carbonate phases: (a) ACC Method II, CP/MAS, 1 ms contact time, 40000 scans; (b) ACC Method I (^{13}C-enriched), SP/MAS, 2 scans; (c) calcite, SP/MAS; (d) monohydrocalcite, CP/MAS, 1 ms contact time; (e) aragonite, SP/MAS; (f) vaterite, SP/MAS. All spectra acquired with 3 kHz spinning rate except (d), 5 kHz. Dotted lines denote the isotropic chemical shifts for comparison.

3.4. NMR of ACC. The ^{13}C NMR spectra for the initial ACC synthesized using methods I and II are virtually identical and are characterized by a broad (fwhh of 3.6 ppm), symmetric peak at $\delta_C = 169 \pm 0.5$ ppm (Figure 7). This feature is essentially identical whether acquired by SP or CP methods. For comparison, Figure 7c−f shows ^{13}C MAS NMR spectra acquired by either SP or CP methods of other calcium carbonate phases, including those for monohydrocalcite (Figure 7d; $\delta_C = 171.7$ ppm, fwhh = 2.3 ppm) and vaterite (Figure 7f; $\delta_C = 170.7$ ppm and 169.6 ppm, fwhh = 0.8 ppm), which have not been reported previously (Supporting Information, Text-5). Dotted lines in Figure 7 represent the chemical shifts for calcite (Figure 7c, $\delta_C =$ 168.7 ppm,) and aragonite (Figure 7e, $\delta_C = 171.0$ ppm,). The large peak width for ACC, which spans the ^{13}C chemical shift range of crystalline calcium carbonates, is much broader than that of the crystalline phases and is consistent with the amorphous nature of the initial ACC.

The $^{13}C\{^1H\}$ CP/MAS signal intensity of ACC varies with contact time (τ_c) according to classical biexponential kinetics [33,34] characterized by $T_{CH} = 0.5$ ms and $T_{1\rho,H} = 5.0$ ms (Supporting Information, Figure S5), with $\tau_c = 1$ ms giving maximum signal intensity. The inferred $T_{1\rho,H}$ from

(33) Kolodziejski, W.; Klinowski, J. *Chem. Rev.* **2002**, *102* (3), 613–628.
(34) Mehring, M. *Principles of high-resolution NMR in solids*; Springer-Verlag: Berlin, 1983; p 342.

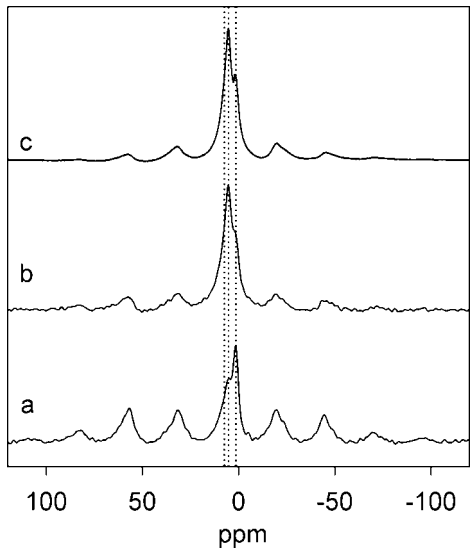

Figure 8. (a, b) HETCOR summed projections acquired with 1 ms contact time and displayed in absolute intensity mode. (b) includes a 50 ms mixing time. (c) ^{1}H single pulse MAS NMR spectrum. All spectra were obtained at 10 kHz spinning rate. HETCOR spectra were summed across the ^{13}C peak from $\delta_C = 170.0$ to 167.5 ppm.

the CP kinetics was confirmed by a ^{13}C-observed ^{1}H $T_{1\rho}$ measurement undertaken at a constant $\tau_c = 1$ ms. In terms of peak position and width, no variation in the ^{13}C CP spectrum was found with contact time.

^{13}C{^{1}H} 2-D HETCOR NMR spectra were obtained to determine the nature of H associated with carbonate in the ACC structure. The ^{13}C dimension of the 2-D contour plot (Supporting Information, Figure S6) shows only the characteristic signal of ACC ($\delta_C = 169$ ppm, fwhh = 3.6 ppm). The ^{1}H slices (F1) across the ACC ^{13}C resonance from $\delta_C = 172$ to 165 ppm are essentially identical so that the ^{1}H sum projection can be used to represent the ^{1}H spectrum arising from hydrogens in close proximity to carbonate. Figure 8a shows the ^{1}H sum projection (from $\delta_C = 170.0$ to 167.5 ppm) from the ^{13}C{^{1}H} HETCOR spectrum acquired with 1 ms contact time, which contains at least three components, including two narrow peaks, at 1.5 ppm and 5.3 ppm, and a broad spinning sideband (SSB) pattern centered at 6 ppm (obtained as the average of the $n = \pm 1$, ± 2 sideband positions). The narrow peak at 1.5 ppm is assigned to OH groups and the peak at 5.3 ppm likely arises from mobile molecular water. The broad SSB pattern indicates the presence of rigid molecular H_2O. ^{13}C{^{1}H} HETCOR spectra with shorter contact time (e.g., 0.2 ms) were also obtained, but the ^{1}H projections are very similar to that obtained at 1 ms contact time. ^{13}C SP NMR spectra acquired before and after each HETCOR experiment of dried ACC showed no evidence of transformation to crystalline phases (Supporting Information, Figure S7). In contrast, peaks from calcite and aragonite are clearly evident within a few hours if the ACC remains exposed to the atmosphere.

To quantify the different ^{1}H-bearing species associated with the carbonate, ^{13}C{^{1}H} HETCOR NMR spectra were obtained with a mixing time (τ_{mix}) added before the contact time. During τ_{mix}, ^{1}H spins in different environments can exchange polarization through the ^{1}H$-^1$H homonuclear dipolar interactions. At long mixing time, the ^{1}H magnetization reaches equilibrium, giving a quantitative and indirectly observed ^{1}H spectrum from the HETCOR experiment, with the ^{1}H intensity of each component proportional to the population of corresponding species. The ^{1}H HETCOR sum projection acquired with $\tau_{mix} = 100$ ms is nearly identical to that with 50 ms mixing time (Figure 8b), indicating the ^{1}H polarization has equilibrated within 50 ms. Therefore, the ^{1}H signal intensities in Figure 8b represent the ratio of different ^{1}H-bearing species near carbonate groups in ACC. Least-squares fits to the spectrum in Figure 8 show that the SSB pattern represents about 40% of the ^{1}H intensity, indicating that a significant fraction of the ^{1}H-bearing species in ACC are present as rigid structural H_2O. This observation suggests that rigid H_2O, which we infer to be coordinated to Ca atoms, and the H-bonding play a crucial role for the formation and stabilization of the ACC structure. The fraction of H present as hydroxyl groups ($\sim 7 \pm 3\%$) is above the defect level, implying the rigid OH groups might also play a role in the ACC structure. Comparison with Figure 8a, for which ^{1}H spin diffusion occurred only during τ_c, shows that with additional mixing time the peak at 5.3 ppm becomes dominant, representing about $55 \pm 5\%$ of the H, while the intensities of SSB pattern and the peak at 1.5 ppm decrease, implying that the ^{1}H signal at 5.3 ppm has a lower CP rate, as would be expected for H_2O molecules undergoing restricted motion. This result is consistent with preliminary variable-temperature experiments, which show that the ^{13}C{^{1}H} CP/MAS intensity increases by a factor of 2 upon lowering temperature to -120 °C to reduce the motion. The ^{1}H single pulse MAS spectrum was also obtained for comparison (Figure 8c), and shows almost the same pattern as the equilibrated ^{1}H HETCOR spectrum (Figure 8b), indicating that all the H are in contact with the ^{13}C-detected, rigid ^{1}H-bearing species. This result indicates that no significant H is present as a separate fluid phase under these conditions. No signal was observed that could be assigned to hydrogen carbonate groups in ACC. The short C$-$H distance of bicarbonate should result in a short T_{CH} values, however no distinct signal was significantly enhanced in CP/MAS spectra at short contact time. We have previously reported hydrogen carbonate defects in calcite, which occur near $\delta_{H\text{-}1} = 7.4$ ppm,[35] but such groups do not appear to be abundant in ACC.

From correlations of ^{1}H NMR chemical shift with hydrogen bond length (e.g., ref 36), an average hydrogen bond length of $d(O\cdots O) = 2.87$ Å can be estimated for the rigid structural water in ACC observed by NMR ($\delta_H = 6$ ppm). This O$-$O distance is in good agreement with a feature near 2.9 Å in the PDF of ACC (Figure 5) which does not occur in calcite, an anhydrous carbonate. A similar feature is observed in the PDF of monohydrocalcite, which arises from $O_{(water)}-O_{(carbonate)}$ correlations, although there is also a contribution near this distance for Ca$-$C correlations from bidentate carbonate configurations (Figure 6). The large difference in the average ^{13}C chemical shift between ACC

(35) Feng, J.; Lee, Y. J.; Reeder, R. J.; Phillips, B. L. *Am. Mineral.* **2006**, *91* (5−6), 957–960.
(36) Yesinowski, J. P.; Eckert, H.; Rossman, G. R. *JACS* **1988**, *110* (5), 1367–1375.

and the phases containing bidentate carbonate (monohydrocalcite and aragonite) suggests that most of the carbonate in ACC is monodentate. In this case, the 2.9 Å correlation should be dominated by O−O correlations, although we cannot rule out the existence of any Ca−C correlations in this range because the large width of the ^{13}C resonance does overlap slightly the peak position for monohydrocalcite and aragonite.

4. Conclusions

By complementing existing approaches with structural methods previously not used, we have provided new insight into structural aspects of hydrated amorphous calcium carbonate formed in vitro. Here we have shown that two different preparation methods for forming ACC yield virtually identical products as determined by PDF, NMR, and EXAFS techniques. The PDF shows that the ACC exhibits short-range and limited intermediate-range order that does not extend beyond 15 Å and therefore can be considered as a truly amorphous solid. NMR results indicate that most of the hydrogen in ACC is present as structural H_2O and that an additional fraction of rigid OH groups ($\sim 7 \pm 3\%$) might also play a role in the ACC structure. However, over one-half of this water exhibits restricted motion on the millisecond time scale which could play a role in the instability of ACC by enhancing transport of Ca and possibly carbonate. These hydrous components are almost certainly coordinated to Ca atoms. Therefore, Ca atoms in the synthetic ACC could be variably coordinated by CO_3, H_2O, and possibly OH groups.

In evaluating the structure of ACC there is a temptation to choose a structural model from among the well-known crystalline phases in the calcium carbonate system (e.g., monohydrocalcite, vaterite, etc.). We show that the experimentally observed PDF for synthetic ACC does not provide a distinct match to any known structure type in the calcium carbonate system. This finding is supported by ^{13}C NMR of ACC, which also shows no correspondence of the average ^{13}C chemical shift to any other calcium carbonate phase. In particular, comparison of the PDFs and NMR spectra for ACC to those of monohydrocalcite indicates that these phases have distinct differences in terms of the distribution of interatomic distances as well as the configuration of carbonate which is predominantly monodentate in ACC versus bidentate in monohydrocalcite. These observations confirm that synthetic ACC is not simply a nanocrystalline or disordered form of monohydrocalcite. Although we argue that it is not prudent to describe ACC using models originally based on structures with infinite periodicity, future studies may reveal more similarities between the structure of ACC and one of these crystalline phases.

Although further work will be necessary to fully understanding the structures of different ACC varieties, the results presented here on synthetic, additive-free ACC provide a baseline for evaluation of biogenic samples as well as synthetic ACC samples containing additives. The unique structural information present in the PDF for ACC is expected to contribute substantially to its structure determination. Studies of dynamic and unstable phases like ACC often benefit from also evaluating inorganically derived materials formed in vitro under controlled laboratory conditions. Such studies enable researchers to remove complexity caused by the presence of multiple impurities such as metals and organics. However, results from studies of synthetic ACC are not necessarily fully applicable to natural systems and this must be taken into consideration when comparing the results presented here to prior related studies.

Acknowledgment. We thank Peter L. Lee, Peter J. Chupas, Mali Balasubramanian, and Steve Heald for assistance with data collection at the Advanced Photon Source, Argonne National Laboratory and Martin A. A. Schoonen for advice and support. We thank Yuanzhi Tang for assistance in sample preparation. Funding was provided by the Center for Environmental Molecular Science (CEMS) and the National Science Foundation (Awards CHE0221934, DMR-045244, and EAR-0510501) and also the U.S. Dept. of Education through the GAANN Program (Sponsor ID P200A060248). NMR instrumentation is supported through CHE 03-21001. X-ray total scattering data were collected at X-Ray Operation and Research (XOR) beamline 1-ID, and XAS data were collected at the PNC/XOR beamline 20-BM, both at the APS at ANL, and use is supported by the U.S. Dept. of Energy, Office of Science, Office of Basic Energy Sciences, under Contract No. DE-AC02-06CH11357. We also thank Lia Addadi for her insightful comments as well as an anonymous reviewer.

Supporting Information Available: Additional details, XRD patterns, FTIR spectra, and TGA for ACC, calculated total and partial PDFs for vaterite and aragonite, $^{13}C\{^1H\}$ CP kinetics data, $^{13}C\{^1H\}$ HETCOR NMR spectrum, and ^{13}C SP/MAS and $^{13}C\{^1H\}$ CP/MAS NMR spectra of ACC, best fit EXAFS results, and supporting references (PDF). This material is available free of charge via the Internet at http://pubs.acs.org.

CM800324V